Research article **Open Access**

Yinping Miao*, Xixi Ma, Yong He, Hongmin Zhang, Xiaoping Yang and Jianquan Yao

Multidimensional microstructured photonic device based on all-solid waveguide array fiber and magnetic fluid

DOI 10.1515/nanoph-2016-0129
Received July 29, 2016; revised September 20, 2016; accepted September 24, 2016

Abstract: An all-solid waveguide array fiber (WAF) is one kind of special microstructured optical fiber in which the higher-index rods are periodically distributed in a low-index silica host to form the transverse two-dimensional photonic crystal. In this paper, one kind of multidimensional microstructured optical fiber photonic device is proposed by using electric arc discharge method to fabricate periodic tapers along the fiber axis. By tuning the applied magnetic field intensity, the propagation characteristics of the all-solid WAF integrated with magnetic fluid are periodically modulated in both radial and axial directions. Experimental results show that the wavelength changes little while the transmission loss increases for an applied magnetic field intensity range from 0 to 500 Oe. The magnetic field sensitivity is 0.055 dB/Oe within the linear range from 50 to 300 Oe. Meanwhile, the all-solid WAF has very similar thermal expansion coefficient for both high- and low-refractive index glasses, and thermal drifts have a little effect on the mode profile. The results show that the temperature-induced transmission loss is < 0.3 dB from 26°C to 44°C. Further tuning coherent coupling of waveguides and controlling light propagation, the all-solid WAF would be found great potential applications to develop new micro-nano photonic devices for optical communications and optical sensing applications.

Keywords: nanophotonic devices; photonic crystal fiber; nanomagnetic fluid.

1 Introduction

As a new type of photonic crystal fiber (PCF), all-solid microstructured fiber shows versatile transmission characteristics and physical phenomena owing to the solid materials periodically distributed in the cladding with different refractive indexes (RI), which is similar to the microstructured fiber with airholes [1–7]. It is easier to splice and couple with conventional single-mode fibers (SMFs) without airhole collapse. According to different transmission mechanisms, an all-solid microstructured fiber could be divided into an all-solid photonic band gap fiber [8], an all-solid Bragg microstructured fiber [9], and an all-solid waveguide array fiber (WAF) [10]. Waveguide array has some basic properties such as energy band structure, brillouin region, and special discrete diffraction characteristic [11]. At present, the investigations of waveguide array are mainly focused on crystal and semiconductor materials with photorefractive effect or other nonlinear effects. The all-solid WAF could tune coherent coupling of waveguides and effectively control light propagation, including mode coupling and discrete diffraction. Because the high and low RI rods using in the WAF have very similar thermal expansion coefficient, it has low sensitivity to temperature. With continuous development of microstructured fiber manufacture technique, the microstructured fiber with two-dimensional waveguide array becomes an attractive research subject. The nonlinear mode-coupling of optical fiber array was used to realize passive mode-locking for the first time [12]. The mode evolution of two-dimensional WAF has been studied theoretically and experimentally [10]. A bending sensor has been

***Corresponding author: Yinping Miao,** Tianjin Key Laboratory of Film Electronic and Communication Device, School of Electronics Information Engineering, Tianjin University of Technology, Tianjin 300384, China; and College of Precision Instruments and Opto-Electronics Engineering, Institute of Laser and Optoelectronics, Tianjin University, Tianjin 300072, China, e-mail: kikosi@126.com
Xixi Ma, Yong He, Hongmin Zhang and Xiaoping Yang: Tianjin Key Laboratory of Film Electronic and Communication Device, School of Electronics Information Engineering, Tianjin University of Technology, Tianjin 300384, China
Jianquan Yao: College of Precision Instruments and Opto-Electronics Engineering, Institute of Laser and Optoelectronics, Tianjin University, Tianjin 300072, China

fabricated based on the interference between different supermodes propagating through waveguide array microstructured fiber [13]. The study on the transmission characteristics of WAF-based fiber Bragg grating has attracted growing research interests recently. Fiber Bragg grating in two-dimensional WAF was fabricated, and it was used to measure curvature and strain [14]. In addition to structure modulation, it is quite important to investigate the interaction between all-solid WAF and external fields, for example, magnetic field.

The light field in optical fiber can be modulated by changing the applied magnetic field intensity. It is also an effective way for magnetic field detection through light field modulation in optical fiber. In recent years, some ways have been proposed, such as multimode fiber with sensitive film coating [15], PCF deposited with Terfenol particles [16], and optical fiber in combination with magnetic fluid (MF) [17, 18]. MF is one kind of magnetic field-sensitive material and has many attractive magneto-optic properties, for example, birefringence property, Faraday property, and magnetic-induced RI tunability [19–22]. It becomes one subject of numerous studies to combine MF with optical fiber for the measurement of external magnetic field [23, 24] and MF birefringence [25]. The magnetic field devices can be constructed by immersing MF as the cladding of a long-period fiber grating [26, 27], by controlling MF coated on subwavelength fiber to realized optical modulator [28], and by using MF as a sensitive medium in fiber optic F-P cavity [29]. Meanwhile, the PCF's cladding airhole is often used as an effective reactor of MF, such as F-P sensor with hollow core PCF [30]. Magnetic measuring equipment was fabricated through filling PCF [31]. Moreover, the magnetic field devices can also be achieved by designing various mode interference structures, including SM-MM-SM, Fabry-Pérot optical fiber interferometer, and Michelson interferometer [32, 33].

In this paper, a multidimensional photonic device was fabricated based on the all-solid WAF with the periodically modulated microstructure formed by electric arc discharge. By combining the microstructure with the MF, we have realized the modulation of light transmission properties in the all-solid WAF as well as the measurement of external magnetic field intensity. The transmission spectral responses of magnetic field and temperature have been experimentally investigated. The results show that the photonic device is sensitive to the external magnetic field but has low sensitivity to temperature. This suggests that the all-solid WAF would find potential applications in the areas of optical communications and optical sensing.

2 Principle and devices fabrication

Figure 1A shows the schematic diagram of the experimental setup for magnetic-field tunability experiment. It consists of two electromagnets, a tunable voltage source (TVS), a supercontinuum broadband source (wavelength ranges from 600 to 1700 nm), and an optical spectrum analyzer (Yokogawa AQ6370C). Electromagnets and TVS are used to produce the magnetic field (H) and to control the intensity of the applied magnetic field. The magnetic field intensity is measured by a Gauss meter with a resolution of 0.1 Gs. Here, we fabricate periodic microstructure tapers along the all-solid WAF axis by using electric arc discharge with a fiber splicer. Two ends of the fiber were fixed on the translation stage; after one tapering is fabricated, the translation stages were moved by a distance of 500 μm along the axis. Such tapering process was repeated five times. Figure 1B shows the cross section of the all-solid WAF. The high RI rods have an average diameter of approximately 7 μm and an interrod spacing (pitch, Λ) of approximately 10 μm. The RI of the high and low glasses is 1.474 and 1.444, respectively. The outer diameter of the all-solid WAF is approximately 124 μm. Figures 1C and D are the microscopic images of one taper and the spacing between two adjacent tapers in the all-solid WAF. The taper length, the waist diameter, and the spacing between two adjacent tapers are ~740, ~78, and ~548 μm, respectively. The actual period of tapers is longer than the distance of translation stages because of the taper-induced elongation of the fiber. The saturable magnetization of the MF (EMG605; Ferrotec, Inc., USA) used in the experiment

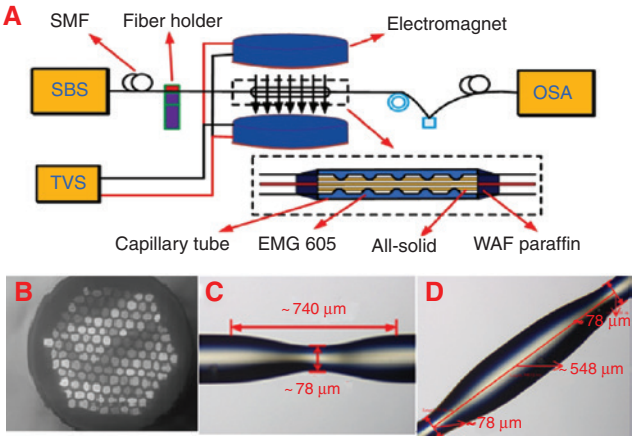

Figure 1: (A) Schematic diagram of the experimental setup for magnetic field tunability experiment. (B) Cross-sectional image of the all-solid WAF. (C) Microscopic image of a typical taper fabricated in the all-solid WAF. (D) Microscopic image of the spacing between two adjacent tapers.

is approximately 300 Oe because of the clustering of the nanoparticles, and the RI of the MF is approximately 1.40 without the external magnetic field. All-solid WAF is spliced between two SMFs and then is immersed into the MF carried by a capillary tube, as shown in the inset of Figure 1A.

Because the rod spacing of the WAF is approximately half of the core diameter of SMF, the central rod of WAF and the first storey high-refractive index rod would be covered with SMF after fusion. When the incident light enters the all-solid WAF from the lead-in SMF, some supermodes will be excited in the all-solid WAF because of the small pitch and the strong energy coupling between high RI rods. In a way, such all-solid WAF can be seen as an RI guiding multimode fiber with its core formed by the high RI rods and the quartz substrate between high RI rods. The residual external quartz substrate could be treated as the fiber cladding. Therefore, these supermodes could be classified according to the mode classification method adopted for conventional step-index optical fibers. Because of the presence of periodic tapers, different supermodes have various propagation constants in the all-solid WAF. The supermodes propagating in cladding will be recoupled back into the SMF core after they propagate a long distance. Therefore, interference will occur among them, and the interference fringes can be observed in the transmission spectra.

The electric field distribution induced by the interference at a propagation distance of L is determined by the following equation [34]:

$$E(r, L) = \sum_{m=1}^{M} a_m E_m(r) e^{i\beta_m L}, \tag{1}$$

where M is the number of total modes in the all-solid WAF, $E_m(r)$ is the electric field profile for each mode of the all-solid WAF, and β_m and a_m are the propagation constant and the excitation coefficient of the mth-order mode, respectively. The excitation coefficient a_m can be written as follows [34]:

$$a_m = \frac{\int_0^\infty E(r, 0) E_m(r) r dr}{\int_0^\infty E_m(r) E_m(r) r dr}, \tag{2}$$

where $E(r, 0)$ represents cross-sectional eigenmode field distribution of the incident light.

When two kinds of modes interfere with each other, the phase difference between the mth mode and the fundamental mode can be approximated as $\phi = 2\pi\Delta n_{\text{eff}} L/\lambda$, where Δn_{eff} is the effective RI difference between the fundamental mode and the mth mode, and λ is the operating wavelength. When the phase difference satisfies the condition that $\phi = (2m+1)\pi$ (m is an integer), the peak wavelength can be expressed as:

$$\lambda_m = \Delta n_{\text{eff}} L / p. \tag{3}$$

Thus, the output light intensity at the out port of the all-solid WAF can be figured out by $I(r, L) = E(r, L)E^*(r, L)$, which can be expressed as follows:

$$I(r, L) = 10\log_{10}\left(\frac{\left| \int_0^\infty E(r, 0) E(r, L) r dr \right|}{\int_0^\infty |E(r, L)|^2 r dr \int_0^\infty |E(r, 0)|^2 r dr} \right). \tag{4}$$

The effective RI of the high-order modes will change with the variation of the ambient RI, which leads to the change of the effective RI difference. The relationship between the propagation constant of the mth mode and the corresponding effective RI can be written as $n_{\text{eff}}^{m\text{th}} = a_m / k_0$, where k_0 is the wave number in free space. Therefore, the propagation constant of the mth mode will alter as well as the ambient RI changes, resulting in the variation of output light intensity $I(r, L)$ according to Equations (1) and (4).

3 Experimental results and discussion

The evolutions of the transmission spectra with the all-solid WAF before and after being periodically tapered are shown in Figure 2. The clear resonance dips turn up after the all-solid WAF is periodically tapered. For the general all-solid WAF, it exits coherent coupling between the core mode and the low-order supermode. After fabricating the periodic tapers, the coupling coefficient between waveguides will change, and the coupling between the core mode and the higher-order supermodes will be produced.

The transmission spectra of the all-solid WAF with periodic tapers before and after immersion into MF without external magnetic field are presented in Figure 3, which indicates the transmission loss increases. This phenomenon is related to the excited supermodes propagating in the refractive rods. After being immersed into MF, the effective RI of cladding mode has increased from 1.0 to 1.4. On the basis of the coupling between the core mode and the different excited high-order modes, different changes of the resonance dips could be observed because of the transformation of Δn_{eff}. Thus, different dips show diversification.

During the magnetic field intensity measurement process, the all-solid WAF is fixed by the fiber holder

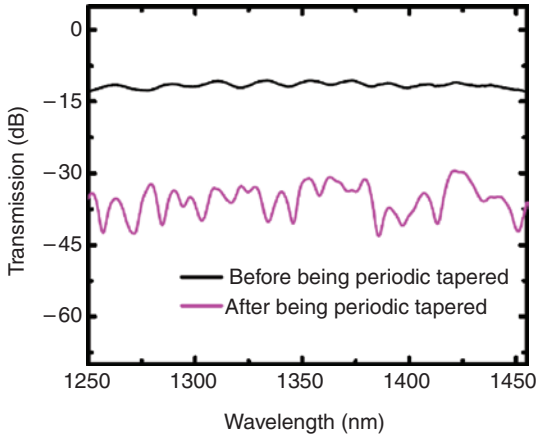

Figure 2: Transmission spectra of the all-solid WAF before and after being periodically tapered.

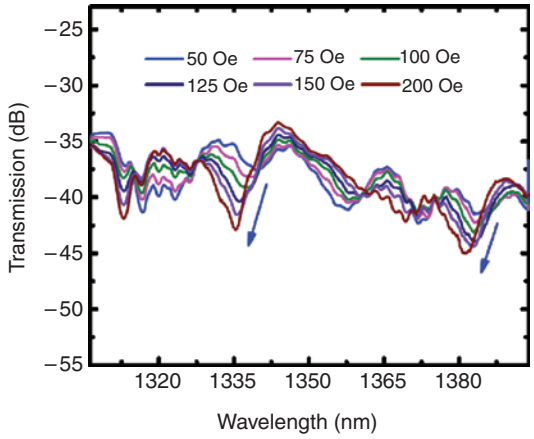

Figure 4: Transmission spectral evolutions of the all-solid WAF with periodic microtapers under different magnetic field intensities.

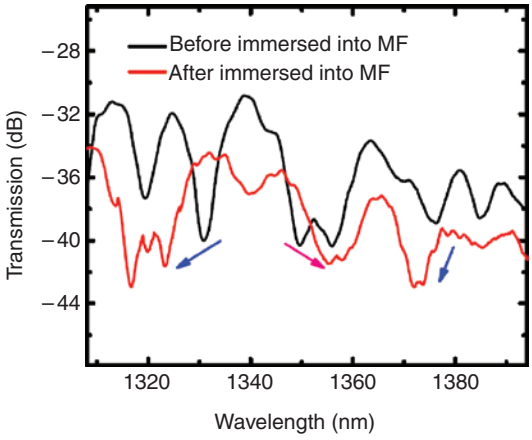

Figure 3: Transmission spectra of the all-solid WAF with five periodic microtapers before and after being immersed into the MF.

and to avoid the strain-induced measurement error. The transmission characteristics are shown in Figure 4. The magnetic field intensity is tuned by the TVS and measured by a Gauss meter. From Figure 4, we can see that the transmission loss increases and the wavelength shows blueshift with the increment of applied magnetic field intensity. The measured result can be explained by the tunable RI (n_{MF}) of the MF. According to the formula $n_{MF} = \sqrt{\varepsilon_r} = \sqrt{1+\chi}$, the electric susceptibility χ of the MF is related to the intensity of the magnetic field and the relative orientation between the electric field E and the magnetic field H as well. χ decreases with the increase of the magnetic field intensity when E is perpendicular to H. χ increases with the increment of the magnetic field intensity, whereas E is parallel to H [25]. Here, the external magnetic field H is applied along the perpendicular direction, whereas the optical electric field E is applied along the fiber axis. Therefore, with the increment of external magnetic-field intensity, the RI of the MF will decrease according to the relative orientation between the electric field E of the light source and H. According to Equations (2) and (4), the a_m will alter and hence excite cladding eigenmodes. The electric field distribution $E(r, L)$ and the output light intensity $I(r, L)$ will change. According to the Equation (3), the transmission spectrum will shift toward the short wavelength region for the high-order mode. The transmission loss keeps constant as the magnetic field intensity is < 50 Oe because of the initial magnetization. When the magnetic field intensity is more than 300 Oe, the transmission loss gradually becomes constant again because of the saturated magnetization of the MF. This phenomenon could be explained by the RI of the MF and the magnetic field intensity satisfying the Langvin function [35]. When an external magnetic field is applied, the magnetic particles dispersed evenly in the MF would agglomerate to form magnetic columns. With the increment of applied magnetic field intensity, some new columns would be formed. Moreover, the agglomerated particles are able to restore to the dispersion state when the applied magnetic field is removed [21, 22]. Therefore, the tapered all-solid WAF has really high repeatability.

Figure 5 shows the relationship between transmission loss and applied magnetic field intensity. The transmission loss increases from − 37.585 to − 50.539 dB by approximately 12.954 dB for an applied magnetic field intensity range of 0 to 500 Oe. In addition, linear fitting shows the magnetic field sensitivity reaches − 0.055 dB/Oe with $R^2 = 0.972$ of the magnetic field intensity between 50 and 300 Oe. The sensitivity to magnetic field could be enhanced by reducing the waist of tapers.

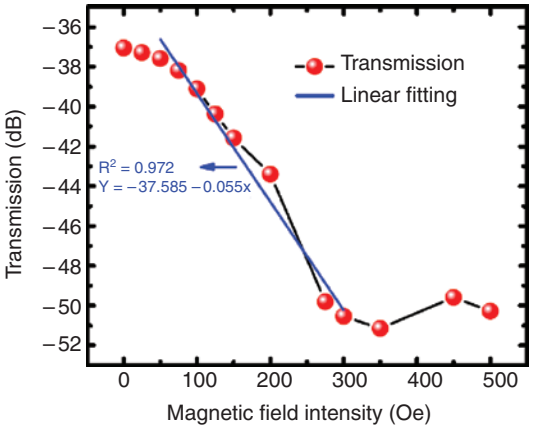

Figure 5: The relationship between transmission loss and applied magnetic field intensity.

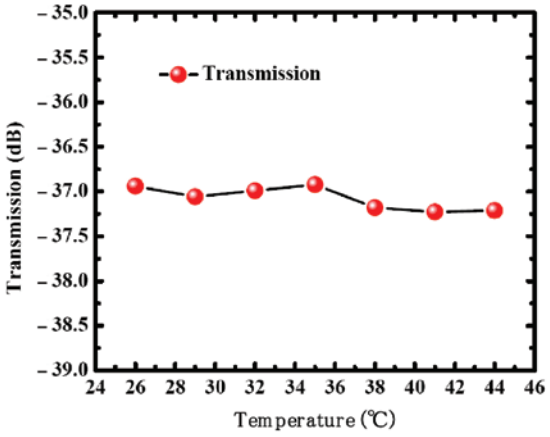

Figure 7: Transmission loss of Dip A as a function of environmental when temperature changes from 26°C to 44°C.

We have also experimentally investigated the temperature effect on the transmission characteristics of the all-solid WAF. It has very similar thermal expansion coefficient for high- and low-refractive index glasses, and thermal drifts have a little effect on mode profile. From Figure 6, the variation of the transmission loss is very weak. As the external temperature increases from 26°C to 44°C, the temperature-induced transmission loss is <0.3 dB, as shown in Figure 7. Because the distribution and the arrangement of magnetic particles in MF change as temperature varies, the effective RI of the MF would change with the variation of environmental temperature. Silica has a thermo-optical coefficient of $+8\times10^{-6}$/°C, whereas the thermo-optical coefficient (-2.4×10^{-4}/°C) of the MF is two orders of magnitude higher [36]. Therefore, the effect of the MF on the silica background could be neglected. The effective RI of the MF changes with the variation of environmental temperature, which leads to the variation of the effective RI of high-order modes. The output intensity $I(r, L)$ would vary with the change of the effective RI of the MF for different environmental temperatures. Also, the magnetically induced RI change of the EMG605 MF is in a magnitude of $\sim5\times10^{-2}$ [37], whereas the corresponding thermally induced RI change of MF is smaller. Thus, the temperature variation of the photonic device has a little effect on the measurement of applied magnetic field intensity. During the entire measurement process, the ambient temperature is kept at a room temperature of 26°C to achieve a highly accurate measurement of external magnetic field, and the effect of temperature fluctuations can be disregarded. In addition, the periodic taper of the device is actually similar to the refractive periodic modulation of long period grating. However, the device with periodic tapers proposed in this paper is symmetrical along the axis. The temperature sensitivity is different from LPG fabricated by the CO_2 laser because the deformation degree of fiber core and cladding is much less than LPG, which is caused by an elasto-optical effect.

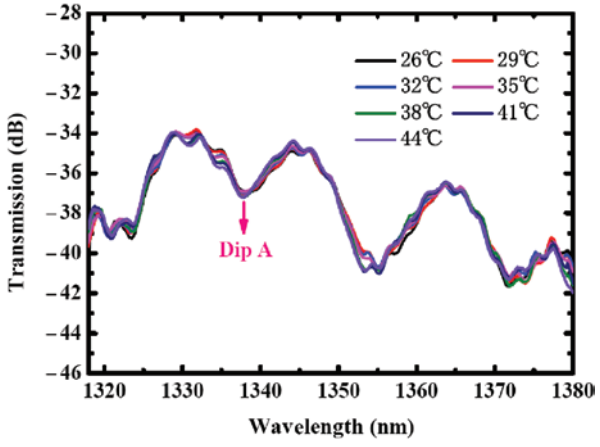

Figure 6: Transmission spectral evolutions of the all-solid WAF under different temperatures.

4 Conclusion

In conclusion, the proposed device combines the radial periodic RI rod distribution of WAF with the axial periodically tapered structure to tune the optical field distribution. A three-dimensional periodically modulated optical field has been fabricated. The transmission spectral characteristics have been investigated under different magnetic field intensities by immersing the all-solid WAF into the MF. As the applied magnetic field intensity increases from 0 to 500 Oe, the wavelength shift is rather small but

the transmission loss increases. The magnetic field sensitivity is – 0.055 dB/Oe for the linear range from 50 to 300 Oe. The temperature effect on the transmission characteristics of the all-solid WAF has been also investigated, and the temperature-induced transmission loss evolution is < 0.3 dB from 26°C to 44°C. Therefore, as a new kind of optical fiber, the all-solid WAF is of significance in fundamental research areas owing to its special structural modulation, repeatability, and fast response.

Acknowledgments: This work was jointly supported by the National Natural Science Foundation of China (grant NOS. 11204212 and 61274113), the Key Natural Science Foundation Project of Tianjin (grant NO. 13JCZDJC26100), and the China Postdoctoral Science Foundation Funded Project (grant NO. 2012M520024).

References

[1] Kuhlmey BT, McPhedran RC, Sterke CMD, Robinson PA, Renversez G, Maystre, D. Microstructured optical fibers: where's the edge? Opt Exp 2002;10:1285–90.
[2] Varshney SK, Fujisawa T, Saitoh K, Koshiba M. Chromatic dispersion profile optimization of dual-concentric-core photonic crystal fibers for broadband dispersion compensation. Opt Exp 2005;13:9516–26.
[3] Poli F, Cucinotta A, Selleri S, Bouk AH. Tailoring of flattened dispersion in highly nonlinear photonic crystal fibers. IEEE Photon. Technol Lett 2004;16:1065–7.
[4] Zu P, Chan CC, Gong TX, Jin YX, Wong WC, Dong XY. Magneto-optical fiber sensor based on bandgap effect of photonic crystal fiber infiltrated with magnetic fluid. Appl Phys Lett 12012;01:241118.
[5] Lin YH, Yang CY, Liou JH, Yu CP, Lin GR. Using graphene nanoparticle embedded in photonic crystal fiber for evanescent wave mode-locking of fiber laser. Opt Exp 2014;21:16763–76.
[6] Liu Y, Wang Y, Sun B, et al. Compact tunable multibandpass filters based on liquid-filled photonic crystal fibers. Opt Lett 2014;39:2148–51.
[7] Brooks CD, Teodoro FD. Multimegawatt peak-power, single-transverse-mode operation of a 100 μm core diameter, Yb-doped rodlike photonic crystal fiber amplifier. Appl Phys Lett 2006;89:111119.
[8] Ding WH, Jiang Y. All-solid photonic band gap fiber based distributed fiber optic pressure sensor. Opt Exp 2012;20:14054–63.
[9] Takashi K, Yuji M, Mitsunobu M. All-solid single-mode Bragg fibers for compact fiber devices. J Lightwave Technol 2006;24:4314–8.
[10] Röpke U, Bartelt H, Unger S, Schuster K, Kobelke J. Two-dimensional high-precision fiber waveguide arrays for coherent light propagation. Opt Exp 2007;15:6894–9.
[11] Christodoulides DN, Lederer F, Silberberg Y. Discretizing light behaviour in linear and nonlinear waveguide lattices. Nature 2003;424:817–23.
[12] Proctor J, Kutz JN. Nonlinear mode-coupling for passive mode-locking: application of waveguide arrays, dual-core fibers, and/or fiber arrays. Opt Exp 2005;13:8933–50.
[13] Li S, Wang Z, Liu Y, et al. Bending sensor based on intermodal interference properties of two-dimensional waveguide array fiber. Opt Lett 2012;37:1610–2.
[14] Wu ZF, Liu YG, Wang Z, et al. Simultaneous measurement of curvature and strain based on fiber Bragg grating in two-dimensional waveguide array fiber. Opt Lett 2013;38:4070–3.
[15] Radojevic V, Nedeljkovic D, Talijan N, Trifunovic D, Aleksic R. Optical fibers with composite magnetic coating for magnetic field sensing. J Magn Magn Mater 2004;272:E1755.
[16] Quintero SMM, Martelli C, Braga AMB, Valente LCG, Kato CC. Magnetic field measurements based on terfenol coated photonic crystal fibers. Sensors 2011;11:11103.
[17] Chen YF, Han Q, Liu TG, Lan XW, Xiao H. Optical fiber magnetic field sensor based on single-mode-multimode-single-mode structure and magnetic fluid. Opt Lett 2013;38:3999–4001.
[18] Li L, Han Q, Liu TG, Chen YF, Zhang RX. Reflective all-fiber current sensor based on magnetic fluids. Appl Phys Lett 2014;85:083107.
[19] Martinez L, Cecelja F, Rakowski R. A novel magneto-optic ferrofluid material for sensor applications. Sens Actuators A 2005;123:438–43.
[20] Zu P, Chan C, Lew WS, Jin Y, Zhang Y, Liew HF. Magnetic-optical fiber sensor based on magnetic fluid. Opt Lett 2012;37:398–400.
[21] Yang SY, Chiu YP, Jeang BY, Horng HE, Hong CY, Yang HC. Origin of field-dependent optical transmission of magnetic fluid films. Appl Phys Lett 2001;79:2372–4.
[22] Yang Y, Chen YF, Horng HE, Hong CY, Tse WS, Yang HC. Magnetically-modulated refractive index of magnetic fluid films. Appl. Phys Lett 2002;81:4931.
[23] Dong SH, Pu SL, Wang HT. Magnetic field sensing based on magnetic-fluid-clad fiber-optic structure with taper-like and lateral-offset fusion splicing. Opt Exp 2014;22:19108–16.
[24] Zheng J, Dong XY, Zu P, et al. Magnetic field sensor using tilted fiber grating interacting with magnetic fluid. Opt Exp 2013;21:17863–8.
[25] Zhao Y, Lv RQ, Li H, Deng QX. Birefringence measurement for magnetic fluid film using optical fiber system. IEEE Photon Technol Lett 2015;27:209–12.
[26] Liu T, Chen XF, Di ZY, Zhang JF, Li XW, Chen JP. Tunable magneto-optical wavelength filter of long-period fiber grating with magnetic fluids. Appl Phys Lett 2007;91:121116.
[27] Yang DX, Du L, Xu ZQ, et al. Magnetic field sensing based on tilted fiber Bragg grating coated with nanoparticle magnetic fluid. Appl Phys Lett 2014;104:061903.
[28] Pu SL, Chen XF, Chen YP, et al. Fiber-optic evanescent field modulator using a magnetic fluid as the cladding. J Appl Physc2006;99:093516.
[29] Zhao Y, Lv RQ, Wang D, Wang Q. Fiber optic Fabry–Perot magnetic field sensor with temperature compensation using a fiber Bragg grating. IEEE Trans. Instrum Meas 2014;63:2210–4.
[30] Zhao Y, Lv RQ, Ying Y, Wang Q. Hollow-core photonic crystal fiber Fabry-Perot sensor for magnetic field measurement based on magnetic fluid. Opt Laser Tech 2012;44:899–902.

[31] Gao R, Jiang Y, Abdelaziz S. All-fiber magnetic field sensors based on magnetic fluid-filled photonic crystal fibers. Opt Lett 2013;38:1539–41.
[32] Deng M, Sun XK, Han M, Li DC. Compact magnetic-field sensor based on optical microfiber Michelson interferometer and Fe_3O_4 nanofluid. Appl Opt 2013;52:734–41.
[33] Wang HT, Pu SL, Wang N, Dong SH, Huang J. Magnetic field sensing based on single mode-multimode-single mode fiber structures using magnetic fluids as cladding. Opt Lett 2013;38:3765–8.
[34] Wu Q, Semenova Y, Wang P, Farrell G. A comprehensive analysis verified by experiment of a refractometer based on an SMF28–small-core singlemode fiber (SCSMF)–SMF28 fiber structure. J Opt 2011;13:125401–6.
[35] Yang SY, Chieh JJ, Horng HE, Hong CY, Yang HC. Origin and applications of magnetically tunable refractive index of magnetic fluid films. Appl Phys Lett 2004;84:5204–6.
[36] Chen YF, Yang SY, Tse WS, Horng HE, Hong CY, Yang HC. Thermal effect on the field-dependent refractive index of the magnetic fluid film. Appl Phys Lett 2003;82:3481–3.
[37] Konstantaki M, Candiani A, Pissadakis S. Optical fibre long period grating spectral actuators utilizing ferrofluids as outclading overlayers. J Eur Opt Soc Rapid Pub 2011;6:11007.